Physica A 559 (2020) 125069

Contents lists available at ScienceDirect

Physica A

journal homepage: www.elsevier.com/locate/physa

Phase diagram for a model of spin-crossover in molecular crystals

J. Quetzalcóatl Toledo-Marín [a,b,*], Carlos Rodriguez [c,d], Yosdel Plasencia Montesinos [d], Gerardo G. Naumis [b]

[a] Biocomplexity Institute and Department of Intelligent Systems Engineering, Indiana University, Bloomington, IN 47408, USA
[b] Departamento de Sistemas Complejos, Instituto de Física, Universidad Nacional Autónoma de México (UNAM), Apartado Postal 20-364, 01000 México, Distrito Federal, Mexico
[c] Faculty of Physics, University of Havana, 10400 Havana, Cuba
[d] Centro de Investigacion en Ciencia Aplicada y Tecnologia Avanzada (CICATA-Legaria), Instituto Politecnico Nacional, 11500 Ciudad de Mexico, Mexico

ARTICLE INFO

Article history:
Received 11 July 2019
Received in revised form 9 July 2020
Available online 20 August 2020

ABSTRACT

Spin-crossover has a wide range of applications from memory devices to sensors. This has to do mainly with the nature of the transition, which may be abrupt, gradual or incomplete and may also present hysteresis. This transition alters the properties of a given sample, such as magnetic moment, color and electric resistance to name some. Yet, a thorough understanding of the phenomenon is still lacking. In this work a simple model is provided to mimic some of the properties known to occur in spin-crossover. A detailed study of the model parameters is presented using a mean field approach and exhaustive Monte Carlo simulations. A good agreement is found between the analytical results and the simulations for certain regions in the parameter-space. This mean field approach breaks down in parameter regions where the correlations and cooperativity may no longer be averaged over.

1. Introduction

Research around several phenomena in the overlap between solid state and condensed matter have the peculiar behavior of having periods of time where it is quite and some other periods of time where a lot of research is being done. Such is the case of spin-crossover (SCO) phenomena, which spans broadly nine decades (see Ref. [1] for a compilation of research over the years together with Refs. [2,3]). The SCO phenomenon is the transition between a low spin (LS) and a high spin (HS) state on a metal ion with $d^4 - d^7$ electronic configuration. Experimental evidence suggest that the cause of this transition has to do with the competition between the strength of the field of ligands and the spin-coupling energy between electrons [4]. For instance, octahedral compounds Transition Metals Series $3d^{4-7}$ present this type of transition, in which they can be in a high or low spin state, depending on whether the ligand field is stronger or weaker than the matching energy.

Furthermore, in the case of thermally induced SCO transition, the free energy difference between both states should be of the order of thermal energy, i.e., k_BT (henceforth we consider $k_B = 1$) [5]. In this sense, high temperature favors

* Corresponding author at: Departamento de Sistemas Complejos, Instituto de Física, Universidad Nacional Autónoma de México (UNAM), Apartado Postal 20-364, 01000 México, Distrito Federal, Mexico.
E-mail addresses: j.toledo.mx@gmail.com (J.Q. Toledo-Marín), crc@fisica.uh.cu (C. Rodriguez), laplace2108@gmail.com (Y. Plasencia Montesinos), naumis@fisica.unam.mx (G.G. Naumis).

https://doi.org/10.1016/j.physa.2020.125069
0378-4371/

HS whereas low temperature favors LS. Interestingly, the phenomenon is rather ubiquitous in nature. For instance, in the case of the transition in Fe^{II} complexes between t_{2g}^6 ($S = 0$) and t_{2g}^6 ($S = 2$) configurations, SCO is responsible for oxygen transport in hemoglobin and probably for the change under pressure of ferropericlase in the Earth's mantle [6]. In solids, SCO can be found in many transition metal oxides, organometallic complexes, inorganic salts or organic radicals and has a cooperative nature, frequently leading to abrupt changes of macroscopic physical properties and hysteresis. Perhaps even more appealing are the applications of SCO which range from display and memory devices and electroluminescent devices to MRI contrast agent [1,7]. Additionally, the use of SCO combined with the properties of nanoporous metal–organic frameworks may also be used in molecular sensing [8].

The HS and LS phases have different properties that depend on the electronic distribution in 3d orbitals. In this sense, the HS to LS transition has a large impact on the physical properties of a material, such as the magnetic moment, the color, the dielectric constant as well as the electrical resistance, among other properties. In other words, features such as optical, vibrational, magnetic and structural differ between one phase and the other. Hence, measuring these properties serve as a proxy to measure and monitor the SCO induced by external perturbation, such as light, pressure or temperature, for instance [9–13]. Several techniques such as magnetic susceptibility measurements, as well as optical and vibrational spectroscopy of the kind of UV, IR, Raman and Mossbauer spectroscopy are used for this end. However, the holy grail is predicting the spin curve for a given material under cooling and heating together with the critical temperature and the hysteresis loop. There has been various efforts in this directions [10,14], yet there is still a lack of a theory, which should not come as a surprise given the great variety of materials having SCO. A complete microscopic description requires the consideration of three basic ingredients: (i) the spin and vibrational states of individual octahedral complexes, (ii) the interaction between them leading to cooperative effects and (iii) the coupling with external factors such as temperature, pressure as well as external electric or magnetic field . In this regard, for instance, in oxides cooperativity is attributed to electronic exchange while in molecular crystals to electron–phonon coupling [15].

In a previous paper by two of the authors [16], a theoretical approach to SCO in mononuclear molecular crystals containing Fe^{II} ions was presented, where a simple effective interaction between neighboring local breathing modes was considered. Only electrons in e_g states are linearly coupled to vibrations, being that the case there is no need for two breathing modes with different vibrational frequencies and coupling parameters. Furthermore, decoupling breathing modes with successive canonical transformations leads to a lattice model where short range and long range ferromagnetic and antiferromagnetic interactions arise in a straightforward manner. In the present paper we further study the phase diagram by means of Monte Carlo simulations and analytical derivations. The structure of the paper is as follows: In the next section we present the model and its features, in Section 3 we solve the model in the thermodynamical limit, in Section 4 we compare the analytics with the simulations and discuss the results, finally Section 5 is for conclusions.

2. Model

Consider a d- dimensional periodic array of i $(1, \ldots, N)$ mono-nuclear metal complexes, each containing an ion Fe^{II} in an octahedral site surrounded by non-magnetic ligands. The number of electrons occupying e_g states at the ith ion will be denoted with n_i which represent the spin on the lattice site i and can take the values 0,1 or 2. We further consider the degeneracy for each state, g_n, such that $g_0 = 1$, $g_1 = 9$ and $g_2 = 15$. In our model we call LS and HS phase the macroscopic state where the mean spin value equals 0 and 2, respectively. In addition, we call intermediate spin (IS) phase the macroscopic state with mean spin value $0 < \langle n \rangle < 2$. Since the charge density distribution of the antibonding e_g states is more localized near their octahedral neighbors, these electrons are strongly coupled with a local breathing vibration mode described by the operators $\hat{a}_i^\dagger$ and $\hat{a}_i$. Here the operator $\hat{a}_i^\dagger$ creates at site i a breathing mode quanta while $\hat{a}_i$ is the corresponding aniquilation operator. Such modes have the following Hamiltonian,

$$\hat{H}_i^{br} = \left(\hat{a}_i^\dagger \hat{a}_i + \frac{1}{2}\right)\hbar\omega, \tag{1}$$

where ω is the frequency of the breathing modes. Here we will measure all energies in terms of such frequency. Thus, in what follows $\hbar\omega$ is set to one.

It has been shown previously that the surrounding ligands have a role in two types of interactions, viz, local vibrations and propagating phonons [17,18].

Given the complex nature of SCO, there is a trade-off between detailed modeling and a basic physical understanding of the phenomenon. Here we tilt the balance towards the latter. In this spirit, we simply hard-wire the ion interaction with the breathing mode at the same site through a coupling parameter α while we also couple neighbor breathing modes through a coupling parameter λ. However, we stress that this coupling parameters contain rich information regarding the physics of the SCO. These coupling parameters in reality are frequency dependent and, thus, phase-dependent [17,18]. Here we use the Hizhnyakov et al. bilinear coupling form where the ion–phonon coupling is taken into account by the interaction of the local vibrations with phonons [19]. The coupling of the electronic shells of the metal ions with the molecular modes is given by the local strain-field written in normal modes $\hat{Q}_i$, and the interaction Hamiltonian is [19,20] $H^{i-br} = -\alpha n_i \hat{Q}_i$. Then $\hat{Q}_i$ is written in terms of the creation/anhilation operators, from where it follows that $\hat{Q}_i = (\hat{a}_i^\dagger + \hat{a}_i)$. Here all constants are absorbed into the coupling α. In a similar way, local breathing modes in neighbor sites will interact

according to the product of normal mode coordinates $\hat{V}_{ij} = \lambda \hat{Q}_i \hat{Q}_j$. Then, the effective Hamiltonian for this electron-local vibrations system is:

$$\hat{H} = \sum_{i=1}^{N} \hat{H}_i + \sum_{\langle i,j \rangle} \hat{V}_{ij} \ , \tag{2}$$

where

$$\hat{H}_i = \epsilon n_i + \left(\hat{a}_i^\dagger \hat{a}_i + \frac{1}{2} \right) - \alpha n_i \left(\hat{a}_i^\dagger + \hat{a}_i \right) \ , \tag{3}$$

is the Hamiltonian for the ith ion, plus the harmonic oscillator that describes breathing modes at the same site, and a term coupling both. Whereas,

$$\hat{V}_{ij} = -\frac{\lambda}{4} \left(\hat{a}_i^\dagger + \hat{a}_i \right) \left(\hat{a}_j^\dagger + \hat{a}_j \right) \tag{4}$$

takes into account the coupling between breathing modes localized in neighbor sites. The parameter $\epsilon > 0$ is the excitation energy per e_g electron, which is obtained by subtracting the splitting energy between t_{2g} and e_g states and the pairing energy P in t_{2g} states. We will assume $\epsilon = 10$ unless stated otherwise explicitly. Moreover, we consider the phonon energy of the local breathing mode when the ion is in HS-state $\hbar\omega = 1$ as well as the Boltzmann constant $k_B = 1$.

Coupling to local modes induces virtual transitions that renormalize electron energies, give rise to an effective electron–electron interaction and shift atomic positions (see below). The interaction Hamiltonian $\hat{V}_{ij}$ is the simplest approximation to an effective inter-site coupling which could result from averaging over degrees of freedom (acoustical phonons) connecting local breathing modes at neighboring sites [18].

As we show in section SN3, by introducing a new set of operators $\hat{c}_{\boldsymbol{q}}^\dagger$ and $\hat{c}_{\boldsymbol{q}}$ obtained through a canonical transformations of $\hat{a}_i^\dagger$ and $\hat{a}_i$, an effective Hamiltonian is obtained in which the ions operators are decoupled from the operators $\hat{c}_{\boldsymbol{q}}^\dagger$ and $\hat{c}_{\boldsymbol{q}}$,

$$\hat{H} = \hat{H}_e + \hat{H}_{ph} \ , \tag{5}$$

where

$$\hat{H}_e = \sum_{i=1}^{N} \left(\epsilon n_i - \alpha^2 n_i^2 \right) - \alpha^2 \lambda \sum_{\langle i,j \rangle} n_i n_j - \sum_{i,j} U_{ij} n_i n_j \ , \tag{6}$$

$$\hat{H}_{ph} = \sum_{\boldsymbol{q}} \sqrt{|1 - \lambda s(\boldsymbol{q})|} \left(\hat{c}_{\boldsymbol{q}}^\dagger \hat{c}_{\boldsymbol{q}} + \frac{1}{2} \right) \ , \tag{7}$$

with effective parameters,

$$U_{ij} = \frac{\alpha^2 \lambda^2}{N} \sum_{\boldsymbol{q}} \frac{s^2(\boldsymbol{q})}{1 - \lambda s(\boldsymbol{q})} e^{i\boldsymbol{q} \cdot (\boldsymbol{R}_i - \boldsymbol{R}_j)} \ ,$$

$$s(\boldsymbol{q}) = \frac{1}{2} \sum_{j(i)=1}^{z} e^{i\boldsymbol{q} \cdot (\boldsymbol{R}_i - \boldsymbol{R}_j)} \ . \tag{8}$$

Here, the notation $j(i)$ and $\langle i, j \rangle$ denote the first neighbor j for a given i and pairwise neighbors, respectively and z is the coordination number, which we assume equal to 6 whenever is not explicitly specified.

Notice that the transformation between the operator a to c given by Eq. (S28) includes the variable n. Therefore, the value of the energy given by Eq. (7) may depend on n. However, we ignore this part, as one can trace out the variable c when the motion of c is much faster than the motion of n.

Thus $\hat{H}_{ph}$ is decoupled from $\hat{H}_e$ and the solutions are not mixed in the Fock space. Such decoupling is achieved by paying the price of having a $\boldsymbol{q}$ dependent effective parameters and an effective ion–ion interaction. As in this representation $\hat{H}_{ph}$ is diagonal, we can concentrate our attention in the pure ion–ion part which will contain the information about phase transitions.

3. Mean field

In this section we present a mean field approximation of the electron–electron Hamiltonian produced in Eq. (6). The idea is to consider first order fluctuations in spins, denoted as δn_i, while neglecting second order fluctuations as in Ref. [21]. To this end, we write $n_i = n - \delta n_i$ where n is the mean value of the spins. It is easy to show that the electron–electron Hamiltonian in Eq. (6) becomes

$$H_e^{mf} = \alpha^2 n^2 \frac{\lambda z}{2} N + \sum_{i=1}^{N} \left(\epsilon - 2n\alpha^2 \frac{\lambda z}{2} \right) n_i - \alpha^2 n_i^2$$

$$+n^2\sum_{i,j}U_{ij}-2n\sum_i\sum_j U_{ij}n_i\ . \tag{9}$$

Notice that under this approach, the spin–spin product between different sites no longer appears and, instead, spins interact with a mean field proportional to $\sim n$. We have also introduced z as the coordination number. Then, computing the partition function using the mean field Hamiltonian, using Eq. (9), is direct, and yields:

$$Z_{mf}=\exp\left[-\beta\left(\alpha^2\frac{\lambda z}{2}N+\sum_{i,j}U_{ij}\right)n^2\right]\times$$
$$\prod_{i=1}^{N}\left(g_0+g_1e^{-\beta\left(\epsilon-2n\left(\alpha^2\frac{\lambda z}{2}+\sum_j U_{ij}\right)-\alpha^2\right)}+g_2e^{-2\beta\left(\epsilon-2n\left(\alpha^2\frac{\lambda z}{2}+\sum_j U_{ij}\right)-2\alpha^2\right)}\right) \tag{10}$$

Notice in the partition function (Eq. (10)) how the dependence on the index i from the product falls with the long range interaction, i.e., U_{ij}. In the case for $N\gg 1$ we may approximate the sum of long range interactions as

$$\sum_{i,j}U_{ij}\approx -N\alpha^2\rho\frac{1}{(1-\frac{1}{\rho})}\ , \tag{11}$$

where we have defined $\rho=\lambda z/2$. The derivation of Eq. (11) is shown in the Supplementary Note (SN) 1.

Hence, using the approximation presented in Eq. (11) we further simplify the partition function to,

$$Z_{mf}=\exp\left[-\beta\frac{n^2\alpha^2\rho N}{1-\rho}\right]\times$$
$$\left(g_0+g_1e^{-\beta\left(\epsilon-\frac{2n\alpha^2\rho}{1-\rho}-\alpha^2\right)}+g_2e^{-2\beta\left(\epsilon-\frac{2n\alpha^2\rho}{1-\rho}-2\alpha^2\right)}\right)^N. \tag{12}$$

From Eq. (12) we may compute any thermodynamic quantity straightforward. Since we are using a mean field approach, the mean field free energy will depend upon the mean spin, n, which is not a proper free energy. Usually the mean-field free energy is larger than the exact free energy.

The mean field free energy per molecule, which we denote as $f_{mf}(n,T)$, is

$$f_{mf}(n,T)=\frac{n^2\alpha^2\rho}{1-\rho}-T\ln\left(g_0+g_1e^{-\beta\left(\epsilon-\frac{2n\alpha^2\rho}{1-\rho}-\alpha^2\right)}\right.$$
$$\left.+g_2e^{-2\beta\left(\epsilon-\frac{2n\alpha^2\rho}{1-\rho}-2\alpha^2\right)}\right)\ . \tag{13}$$

Similarly, in the case where we neglect long-range interactions, i.e., when $U_{ij}=0$ for all i,j, it is not difficult to realize that the mean field free energy, $f_{mf}^{SR}(n,T)$, yields:

$$f_{mf}^{SR}(n,T)=n^2\alpha^2\rho-T\ln\left(g_0+g_1e^{-\beta\left(\epsilon-\alpha^2(2\rho n+1)\right)}\right.$$
$$\left.+g_2e^{-2\beta\left(\epsilon-\alpha^2(2\rho n+2)\right)}\right)\ . \tag{14}$$

The resulting free energies Eqs. (13) and (14) can be readily compared with a recent calculation of the mean field free energy in a SOC homogeneous single-layer molecular compound [22]. Our free energy is basically the same provided that one spin state is neglected, the ground energy is shifted by a constant $-\Delta$, the distance between the LS and HS is set to $\epsilon=\Delta$ and the local spin at each site i to $S_z^i=n_i^i-1$. This results in a constant energy shift and displacement in the magnetization when both free energies are compared. In Ref. [22], the coupling between neighboring spins is given by a parameter (J). Here we show that such coupling comes out as an effective combination of the local normal mode-electron coupling α and the coupling λ between different sites, i.e., $J=2\alpha^2\rho/(1-\rho)z$. Therefore, if the IS states is neglected, the thermodynamics is similar although the cooperativity factor λ leads to a global scaling of the phase diagram . In the following we will explore the parameter space where our model is thermodynamically stable.

Notice from Eqs. (13) and (14) that for $\rho\ll 1$, it follows $f_{mf}\approx f_{mf}^{SR}$. Conversely, under the mean field approximation when $\rho>1$ the long range interaction does not decay with distance. Hence, this imposes a constraint over the system which makes it impossible to draw conclusions from a mean field approach and, in fact, we shall see that the system is highly size-dependent (see SN 1). In fact, if ρ is large enough, the phonon subsystem is unstable and there should appear some lattice distortions that reduce the elastic energy. Thus, the conclusions about this regime are unreliable unless such distortions are included in the model.

Now, in the case of high temperatures, i.e., $T \gg \epsilon - 2n\alpha^2\rho/(1-\rho)$, the mean field free energy, Eq. (13) becomes

$$f_{mf}(n,T) \approx \epsilon\eta - \frac{\alpha^2\rho}{1-\rho}\left(\eta^2 - (n-\eta)^2\right) - \alpha^2\sigma^2 - T\ln\sum_{i=0}^{2} g_i \,, \tag{15}$$

with $\eta = \sum_{i=0}^{2} g_i n_i / \sum_{i=0}^{2} g_i$ and $\sigma^2 = \sum_{i=0}^{2} g_i n_i^2 / \sum_{i=0}^{2} g_i$ being the high temperature mean spin and variance, respectively. Notice that the previous Eq. (15) has a minimum at $n = \eta$ provided $\rho < 1$. Moreover, this is in agreement with the fact that for small values of ρ, $f_{mf} \approx f_{mf}^{SR}$ and in the case of short range interactions, at high temperatures the system must behave as a set of uncoupled spins. This implies that the mean spin is given by $\sum_{i=0}^{2} p_i n_i$, where $p_i = g_i / \sum_{m=0}^{2} g_m$ is the probability obtained simply from the degeneracy of each configuration neglecting any coupling in the model.

It is also worthwhile to compare the analytical results of the present work with those reported in Ref. [23] for a phenomenological approach to cooperativity at the antiferromagnetic quantum critical point of a two-dimensional metal. At this fixed point the strong coupling is unequally felt: the bosonic collective mode is heavily dressed by interactions with the electrons while the electron is only marginally renormalized [23]. In our work, after all the simplifications for the short-range interactions limit, we see that the free energies are only marginally different from the bare result.

For $\rho > 1$, the point $n = \eta$ in Eq. (15) becomes a maximum and the global minimum is located at $n = 0$, i.e., at high temperatures the mean spin becomes zero. In the SN 1 we show that, in fact, for $\rho > 1$ the long range interactions go as $N^{1/4}\exp(N)$, hence any mean field approach fails in describing the model in this parameter region. Henceforth, we consider $\rho < 1$ otherwise specified.

Critical temperature

In this section we compute the critical temperature, which we will denote as T_c. In particular, we show that at low temperatures, there are some parameter values in which the system is equally likely to have a transition where all spins are 2 or 0. In this case, we denote the critical temperature as T_f, to distinguish from a more general case. To understand this, let us consider the mean field free energy in the case of short range interactions (Eq. (14)). The procedure is the same for the case of long range interactions (Eq. (13)). To show this feature in our model, we must prove that for a given set of parameters, there is a critical temperature, T_f, where the mean field free energy has two minima, namely, at $n = 0$ and $n = 2$ such that $f_{mf}^{SR}(0,T_f) = f_{mf}^{SR}(2,T_f)$ and also the global maximum value in the mean field free energy is of the order of T_f, i.e., $T_f \approx \max_n f_{mf}^{SR}(n,T_f)$. Rather than dealing with the cumbersome Eq. (14), we do the following: Notice that the exponentials inside the logarithm in Eq. (14) may go to zero or infinity for low temperatures depending on the values of the parameters as well as the mean spin. Let us consider low temperatures and that $n < (\epsilon - 2\alpha^2)/2\rho\alpha^2$. Then, for low temperatures, we may approximate Eq. (14) with solely the first term. Similarly, in the case where $n > (\epsilon - 2\alpha^2)/2\rho\alpha^2$ we may approximate Eq. (14) thus to write:

$$f_{mf}^{SR} \approx \begin{cases} n^2\alpha^2\rho \,, & \text{for } n < (\epsilon - 2\alpha^2)/2\rho\alpha^2 \\ (n-2)^2\alpha^2\rho + 2\epsilon - T\ln g_2 - 4\alpha^2(1+\rho) \,, & \\ \quad \text{for } n > (\epsilon - 2\alpha^2)/2\rho\alpha^2 \end{cases} \tag{16}$$

In Fig. 1(a) we show the comparison between Eq. (14) and the approximation (16) for some fixed parameter values. Now, given we are using mean field, the minima of the mean field free energy should correspond with the actual free energy. Thus, we should expect that the system is likely to choose low or high spin for the same given parameter-set when two things are fulfilled, namely,

- The mean field free energy at low spin is equal to the mean field free energy at high spin.
- The temperature is of the order of the maximum of the free energy.

The first condition translates into equating Eq. (16) for $n = 0$ with itself for $n = 2$ and solve for the temperature T_f. From this we obtain the temperature $T_f = 2\left(\epsilon - 2\alpha^2(1+\rho)\right)/\ln g_2$. The second condition implies that T_f should be of the order of the maximum value in the free energy. In Fig. 1(b) we have plotted the mean field free energy (Eq. (16)) at temperature $T = T_f$ as well as the temperature T_f for a given set of parameters (see caption), in particular, we fixed $\alpha \approx 1.57$. Notice that the maximum of the free energy is of the order of the temperature which is $T_f \approx 1.0$. As we will see later, the numerical simulations yield a critical temperature of ≈ 1 for the same parameter values.

The straightforward approach to compute the critical temperature T_c consists in finding the temperature where the free energy minima shifts. However, since T_f is, in fact, a critical temperature at which the system is equally likely to become HS or LS, we compute the critical temperature using the same approach we used to obtain T_f: first, we locate the intersection between Eq. (16) when $n < (\epsilon - 2\alpha^2)/2\rho\alpha^2$ and itself when $n > (\epsilon - 2\alpha^2)/2\rho\alpha^2$. Let us denote this intersection as $n_{int}(T)$. It is a feasible task to obtain

$$n_{int}(T) = \frac{2\epsilon - 4\alpha^2 - T\ln g_2}{4\alpha^2\rho} \,. \tag{17}$$

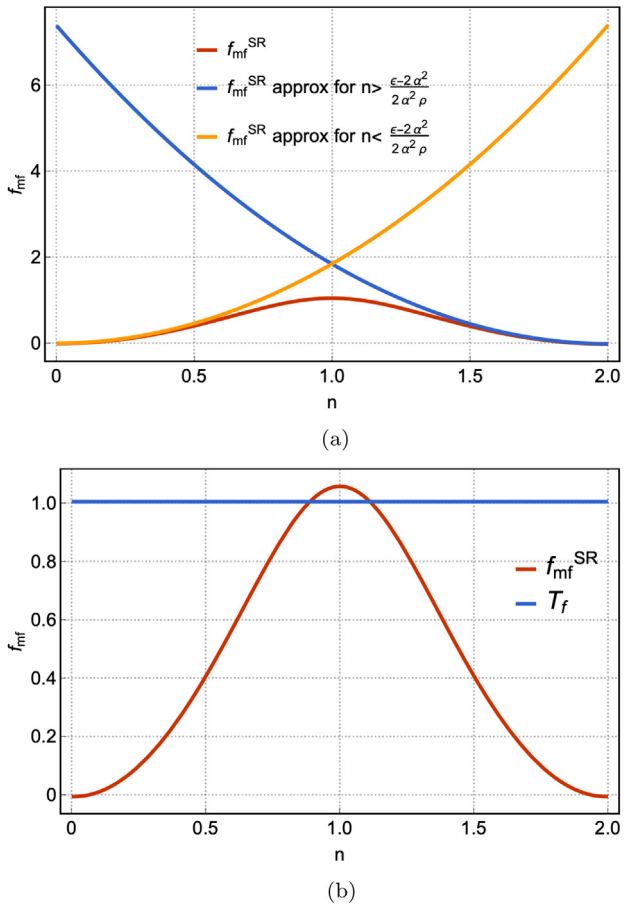

Fig. 1. *(a)* Comparison between the mean field free energy (Eq. (14)) and the approximation at low temperatures (Eq. (16)) *vs.* n. We have fixed the values $z = 6$, $\epsilon = 10$, $T = 1$, $\alpha = 1.57$ and $\lambda = 0.25$. *(b)* Mean field free energy (Eq. (14)) evaluated at the temperature T_f which guarantees that low spin and high spin have the same free energy. The plot also shows T_f for a fixed parameter set $z = 6$, $\epsilon = 10$, $\alpha = 1.57$ and $\lambda = 0.25$. Notice that $T_f \sim f_{mf}^{SR}(T_f)$, which allows the system to choose between low spin or high spin.

Then, solving for T the Eq.

$$T_c = f_{mf}^{SR}(n_{int}(T_c), T_c)\,, \tag{18}$$

yields the critical temperature T_c. In Fig. 2(a) we have plotted the critical temperature *vs.* α from which one may appreciate that T_c decreases as α increases, this is qualitatively consistent with the numerical simulations to be discussed in the next section. We stress that the approach in Eq. (18) is convenient to find a closed expression for the critical temperature in the region around the point where the transition to LS and HS is equally likely, modulated by the α parameter and works provided the low temperature approximation (Eq. (16)) holds.

We now show the transition to LS and HS dependence with α. This is done by noticing that if the intersection between Eq. (16) when $n < (\epsilon - 2\alpha^2)/2\rho\alpha^2$ and itself when $n > (\epsilon - 2\alpha^2)/2\rho\alpha^2$ happens at $n > 1$ then the mean field free energy has a minimum at $n = 0$. Conversely, if it happens at $n < 1$ then the minimum occurs at $n = 2$. In Fig. 2(b) we have plotted $n_{int}(T_c)$ *vs.* α. Notice that for $\alpha < 1.57$ the system goes to LS while for $\alpha > 1.57$ the system goes to HS. However, for $\alpha \approx 1.57$ the system is likely to go HS or LS.

A similar analysis may be done in case of $\rho < 1$ with long range interactions and the outcome is essentially the same. However, the critical temperature is somewhat higher than when neglecting long range interactions. In particular, for $\rho = 0.75$ and $\alpha \approx 1.00$ at $T \approx 1.41$ the system is equally likely to go to LS and HS.

For the case of the IS we will show that it is only possible at high temperatures. For this purpose we use the first and second derivative of the mean field free energy (Eq. (13)). The extremum condition is met provided,

$$T = T_{IS} \equiv \frac{2\left(\epsilon - \frac{2\alpha^2\rho}{1-\rho} - 2\alpha^2\right)}{\ln\left(g_2/g_1\right)}\,. \tag{19}$$

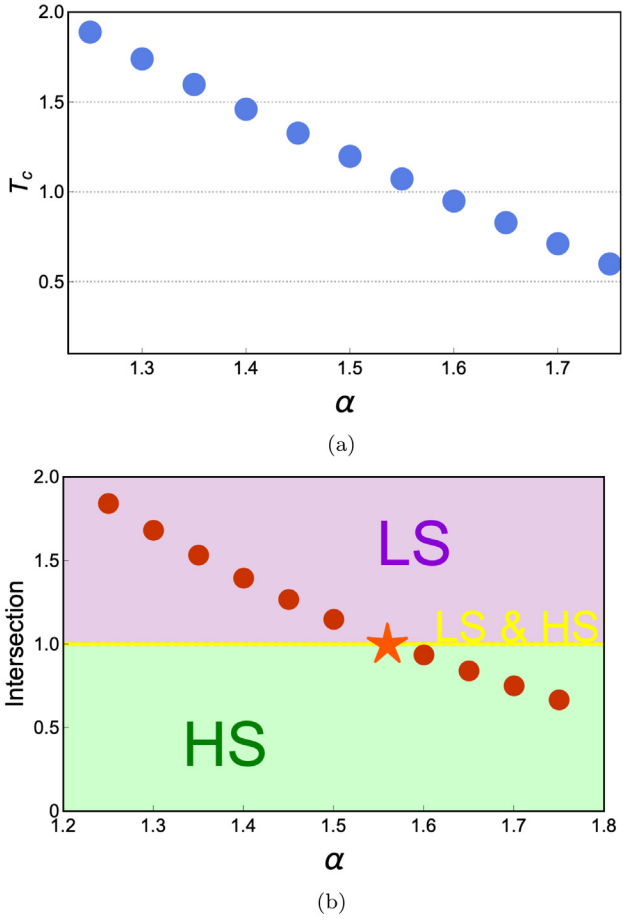

Fig. 2. **(a)** Plot of the critical temperature T_c *vs.* α obtained as described in the text in the mean field approximation neglecting the long interactions (Eq. (13)). **(b)** Plot of $n_{int}(T_c)$ (Eq. (17)) *vs.* α. When $n_{int}(T_c) > 1$ the system goes to LS when the transition occurs. On the contrary, when $n_{int}(T_c) < 1$ the system goes to HS configuration when the transition occurs. When $n_{int} = 1$ the system may go to LS or HS (see main text). The rest of the parameters were kept fixed at $\epsilon = 10$ and $\rho = 0.75$.

Imposing Eq. (19) on the second derivative of Eq. (13) with respect to n and after some algebra we obtain:

$$f_{mf}(n=1,T_{IS}) = \begin{cases} \max, & f_{mf}(n=1,T_{IS}) > u_0 - T_{IS}\ln\frac{4u_0g_0}{T_{IS}} \\ \min, & f_{mf}(n=1,T_{IS}) < u_0 - T_{IS}\ln\frac{4u_0g_0}{T_{IS}} \end{cases}, \tag{20}$$

where $u_0 = \alpha^2\rho/(1-\rho) > 0$. In Fig. 2(b) we have plotted Eq. (19) against α for different values of ρ, while the dashed curve, which is obtained from Eq. (20), represents the boundary between the IS and non-IS phases.

Notice that for low temperatures, the phase $n = 1$ is a maximum while $n = 0$ or 2 is a minimum. The nature of the locality will depend upon the parameters and the temperature. In Fig. 3 (b-d) we have plotted the short-range mean field free energy against n for a fixed set of parameters ($\epsilon = 10$, $\alpha = 1.59$ and $\rho = 0.75$) and different temperatures, also shown in each plot as a dashed line. At high temperatures (Fig. 3(b)) f_{mf} has a local minimum and a global minimum. As temperature decreases, the f_{mf} maximum is of the order of T. This leads to a metastable state associated with the local minimum. As temperature further decreases, the local and global minima swap but at this point the f_{mf} maximum is larger than T and the system gets stuck in the local minimum. We show how this happens in the simulations presented and the next section. When the system has a metastable state and a global minimum, it behaves as a two-level system in which the potential barrier height, the energy and the local curvature of the minima determine the dynamics and hysteresis [24,25].

4. Discussion

In this section we compare the mean field results with the numerical simulations of $\hat{H}_e$ in Eq. (6). In particular, we show that our MC simulations have a phase transition at $T = T_c$. Additionally, depending on the actual value of α, the

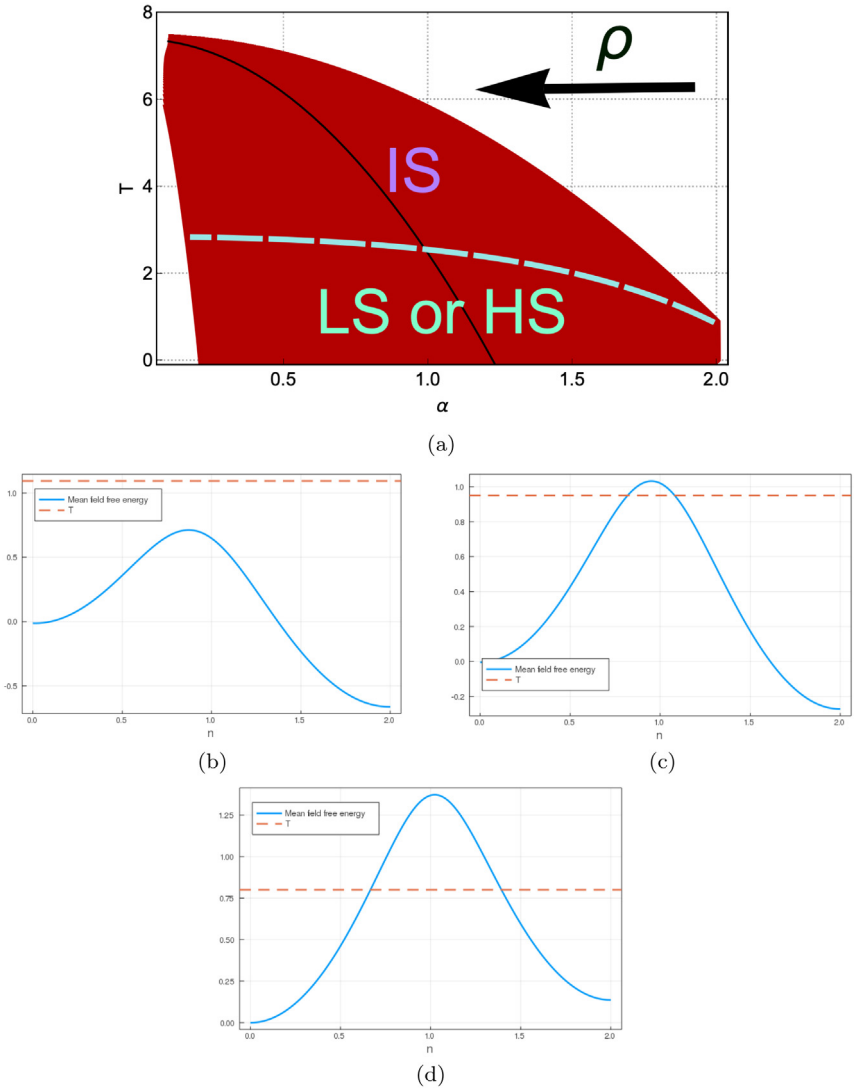

Fig. 3. **(a)** Plot of the temperature $T = T_{IS}$ as a function of α for different values of ρ which increases from right to left (see legends) and $\epsilon = 10$. For exposition purposes, in black we show one of the family curves corresponding to $\rho = 0.70$ for the long range interaction case. The light green dashed curve denotes the transition where the mean field free energy at $n = 1$ changes convexity. Above this curve the system can be in the intermediate phase while below the curve this point becomes a maximum, thus the system can only be in LS or HS. This was obtained from Eqs. (19) and (20). **(b)** Plot of the short range mean field free energy vs n at a temperature higher that the f_{mf} maximum value. **(c)** As the temperature decreases, the mean field free energy maximum is of the order of the temperature, leading to a metastable state and a global minimum. **(d)** As temperature decreases, the global minimum becomes a local one but the temperature is lower than the global maximum leaving the system stuck in this local minimum. We fixed $\rho = 0.75$ and $\epsilon = 10$.

phase transition will be to LS or HS and for a certain window value of α the system can either become LS or HS. Our simulations were done in C++ and Julia [26] using a Monte Carlo algorithm with a Metropolis test [27] for system sizes 10^3, 15^3, 20^3 and 100^3 spins with periodic boundary conditions. To incorporate the long range interactions U_{ij} in our simulations we used the method propose in Ref. [28] and further described in SN2. We fixed the parameters $\epsilon = 10$ and $z = 6$ while considering, both, $\lambda = 0.25(\rho < 1)$ and $\lambda = 0.5(\rho > 1)$ and then for a given fixed set of the previous values we fixed α in the range from 0.1 to 3.0 in the simulations performed in Julia, while in the simulations performed in C++ we increased that range to 4.0. We initiate the simulations at $T_{in} = 15$ with all spins having a value equal to 2. Then, we start lowering the temperature in steps of $\Delta T = 0.25$ and $\Delta T = 1.0$ in the numerical simulation done in C++ and Julia, respectively, until reaching $T \approx 0$.

Now, in Fig. 4 we show contour plots of the mean field Eqs. (13) and (14) for different values of α and λ in a T-n diagram. As was discussed in the previous section, the mean field approach predicts that, in the thermodynamic limit, when long range interactions are considered and $\rho < 1$ for $\alpha = \sqrt{\epsilon/2(1-\rho)}$ the free energy is the same for LS and HS

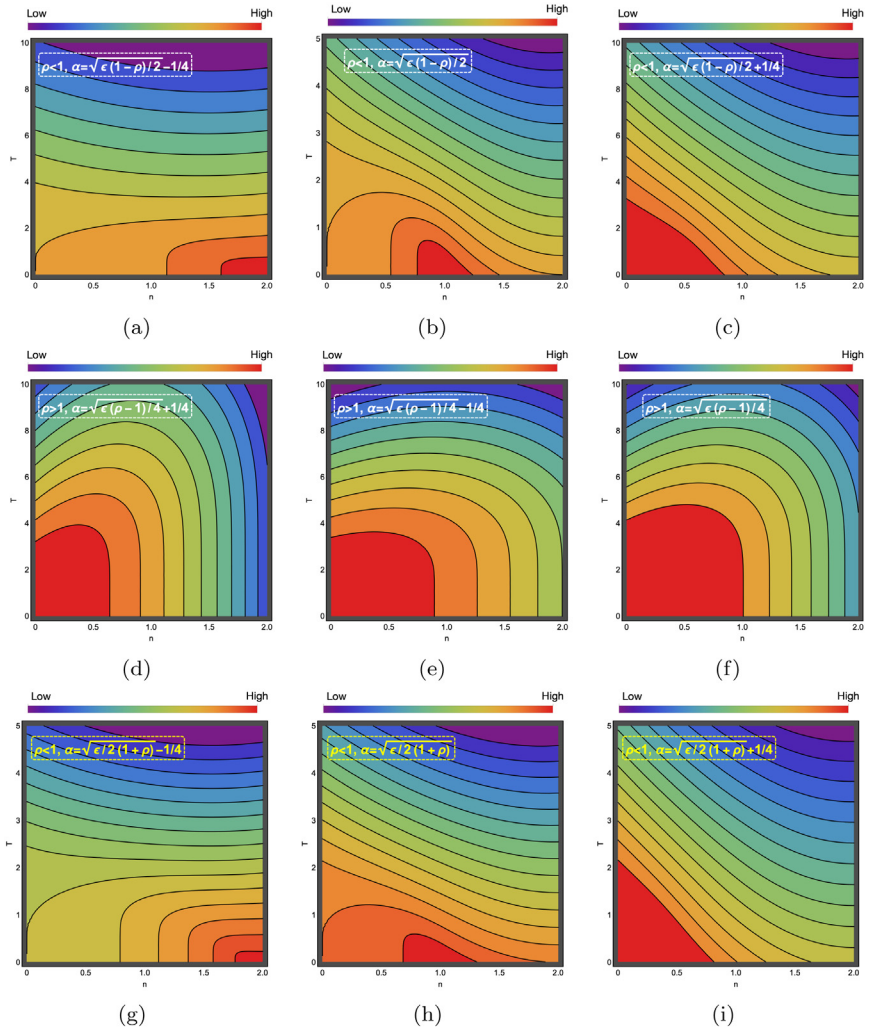

Fig. 4. Mean field free energy per molecule contour plot as a function of temperature and spin, at low temperatures. We have fixed the values $z = 6$, $\epsilon = 10$. **(a–c)** Mean field free energy considering long range interactions (Eq. (13)) with $\lambda = \{0.25\}$ and $\alpha = \{\alpha_0 - 1/4, \alpha_0, \alpha_0 + 1/4\}$ (see captions). **d–f** Mean field free energy considering long range interactions (Eq. (13)) with $\lambda = 0.5$ and $\alpha = \{\sqrt{\epsilon(\rho-1)/4} - 1/4, \sqrt{\epsilon(\rho-1)/4}, \sqrt{\epsilon(\rho-1)/4} + 1/4\}$ (see captions). **(g–i)** Mean field free energy neglecting long range interactions (Eq. (14)). We fixed $\lambda = 0.25$ and consider $\alpha = \{\alpha_0 - 1/4, \alpha_0, \alpha_0 + 1/4\}$ (see captions). α_0 is obtained from solving $n_{int}(T = 0) = 1$ (see Eq. (17) for the case of short-range interactions) for α. The cases where $\rho > 1$ are thermodynamically prohibited since at very high temperatures the equilibrium configuration corresponds to an entropy-minimized configuration (see text for discussion), yet we consider those cases here for completeness.

state as shown in Fig. 4(b). Similarly, when long range interactions are neglected for $\alpha = \sqrt{\epsilon/2(1+\rho)}$ the free energy is the same for LS and HS state as shown in Fig. 4(h). As a matter of completeness we also show contour plots in the case of long range interactions and $\rho > 1$ (Fig. 5(d-f)). Notice that the global minimum is always at $n = 2$. In Fig. 5 we have plotted the mean spin obtained from the simulations, which we denote as, $\langle n \rangle$ *vs.* temperature for the aforementioned case obtained from the simulations. Notice that the black data points in Fig. 5(a), corresponding to $\alpha = 1.5$, show mean spin equal to 0 at low temperatures. Conversely, the black data points in Fig. 5(b) show mean spin equal to 2 at low temperatures and also correspond to $\alpha = 1.5$, i.e., for the same parameter values the system is equally likely in having mean spin equal to 2 as well as equal to 0. This is in excellent agreement with the mean field Eq. (13) where we obtained the value $\alpha \approx 1.57$ summarized in Table 1 and has also been plotted in Fig. 2(b). We have summarized all this in Table 1.

In Fig. 6 we show the mean spin $\langle n \rangle$ *vs.* temperature obtained from our simulations for different system sizes and parameter values which are specified in the legend of the figure. Fig. 6**(a)** to **(c)** correspond to $\epsilon = 10$, $z = 6$ and $\lambda = 0.25$ neglecting long range interactions while considering different system sizes specified in the legends of each plot. Each curve corresponds to a fixed value of alpha that spans from 0.1 to 4.0 (Fig. 6(m) shows the color code we are using), as was described in detail at the beginning of this section. The first thing to notice is that for the system size we are considering, the results are robust. Secondly, notice that although initially all spins have values equal to 2, after

Table 1
Mean spin at low temperature.

(a) Considering long range interactions		
α	ρ	n
$< \sqrt{(2\epsilon - T_f \ln(g_2))(1-\rho)/4}$	<1	0
$> \sqrt{(2\epsilon - T_f \ln(g_2))(1-\rho)/4}$	<1	2
$= \sqrt{(2\epsilon - T_f \ln(g_2))(1-\rho)/4}$	<1	0 or 2
For all values	>1	2
(b) Without long range interactions		
α	ρ	n
$= \sqrt{(2\epsilon - Tf \ln(g_2))/4(1+\rho)}$		0 or 2
$> \sqrt{(2\epsilon - Tf \ln(g_2))/4(1+\rho)}$		2
$< \sqrt{(2\epsilon - Tf \ln(g_2))/4(1+\rho)}$		0

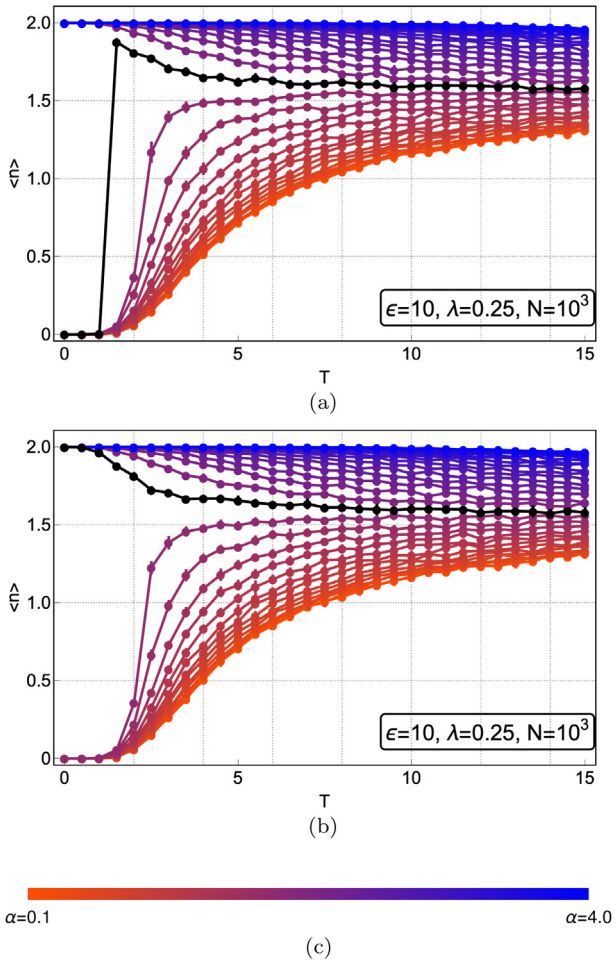

Fig. 5. Mean spin *vs.* T obtained from the simulations. We have fixed the values $z = 6$, $\epsilon = 10$ and $\lambda = 0.25$. The black data points correspond to $\alpha = 1.5$. Notice that in panel *(a)* the magnetization is zero at low temperatures, while in panel *(b)* the magnetization is 2, i.e., the system is equally likely to yield magnetization equal to 0 or 2, in agreement with the mean field prediction (Eq. (13)).

the system is equilibrated the mean spin value ranges from ~ 1.25 for low α-value, to 2.0 for high α-value. Finally, the black data points correspond to $\alpha \approx 1.5$, that is the value predicted by mean field theory where the system can go to spin 0 or spin 1. Fig. 6**(d)** to **(f)** correspond to $\epsilon = 10$, $z = 6$ and $\lambda = 0.5$ neglecting long range interactions while considering different system sizes specified in the legends of each plot. The black data points correspond to $\alpha = 1.2$.

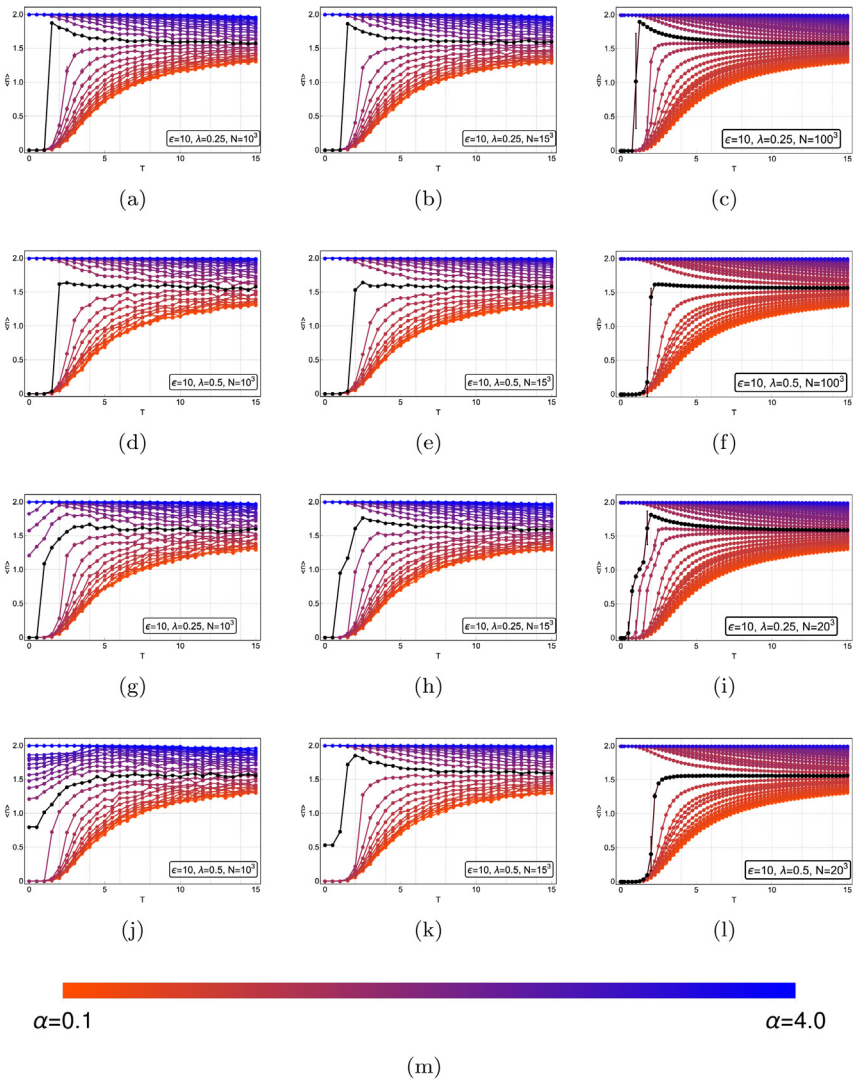

Fig. 6. Mean spin *vs.* T obtained from the simulations. The system size increases from left to right (as specified in each legend). We have fixed the values $z = 6$, $\epsilon = 10$. In **(a-f)** long-range interactions were not considered, while in **(g-l)** long-range interactions were considered. Different values of λ are shown in each plot legend. Each curve corresponds to a given value of α which spans from 0.1 to 4.0. The black data points correspond to a certain α-value in the range $\sim 1.0 - 1.5$ (see main text for discussion). The subpanels **(j-l)** correspond to the thermodynamically unstable.

The mean field approach predicts that for $\alpha \approx 1.3$ the system may go to spin 2 or 0 and $T_f \approx 1.23$, which is consistent with these simulation results. Altogether, for the parameter values considered, the comparison between the mean field approach and the simulation results work well. Besides, the critical temperature predicted by the mean field approach is close to the values obtained in the Monte Carlo simulation, though it is advisable to not relay in mean field approaches to compute such quantities, in general.

Although in real systems the long range interactions will produce lattice distortions, it is interesting to compare the resulting Monte Carlo Simulations since the results are not as obvious as those predicted from the mean field approach. Fig. 6**(g)** to **(i)** correspond to $\epsilon = 10$, $z = 6$ and $\lambda = 0.25$ considering long range interactions as well as different system sizes specified in the legends of each plot. The first thing to notice is that the results obtained in the case where $N = 10^3$ does not match those obtained in the case where $N = 20^3$, thus a bigger system size is required for results to converge to the thermodynamical limit.

Finally, Fig. 6**(j)** to **(i)** correspond to $\epsilon = 10$, $z = 6$ and $\lambda = 0.5$ considering long range interactions as well as different system sizes specified in the legends of each plot. Notice that the results are profoundly system size dependent, which is why mean field approaches are fruitless (see SN 1).

5. Conclusions

In this work we have studied the spin-crossover transition using a simple model derived from quite general assumptions. We have presented a thorough discussion on the parameter space using a mean field approach and Monte Carlo simulation. Using the mean field we were able to obtain the critical temperature where the system can become LS, HS or both. The main result presented here is that when long range interactions are considered and $\rho < 1$, a rescaling of the critical temperature is found. We also found a new phase with $n = 1$ which yet has not been experimentally observed.

When long range interactions were neglected, the mean field critical temperature compared well with the Monte Carlo simulation results. We further showed, both, through the mean field approach and the Monte Carlo simulations that for a small region in the parameter space, at low temperature the model may be in LS or HS state. Although lattice distortions are expected, here we did not considered such effects. However the mean field approach loses accuracy compared to our numerical results as expected due to the increased cooperativity. We further showed that when this happens, the spin *vs.* T curve is highly system size dependent. We also showed that metastable states arise in the model and thus there are hysteresis effects. As happens in rigidity theory of glass transition [29], the present model reinforce the idea that low-frequency phonon and bistable phason modes are essential to describe the phase diagram of a system [30–32]. This means that lattice distortion effects due to long range interactions can be important but we leave this point for future work.

CRediT authorship contribution statement

J. Quetzalcóatl Toledo-Marín: Solved the model, Performed the simulations, Analyzed the results, Wrote the manuscript. **Carlos Rodriguez:** Conceptualized the problem, Proposed the model, Solved the model, Analyzed the results, Wrote the manuscript. **Yosdel Plasencia Montesinos:** Conceptualized the problem, Analyzed the results. **Gerardo G. Naumis:** Solved the model, Analyzed the results, Wrote the manuscript.

Declaration of competing interest

The authors declare that they have no known competing financial interests or personal relationships that could have appeared to influence the work reported in this paper.

Acknowledgments

We gratefully thank DGAPA-PAPIIT project IN102620. J.Q.T.M. acknowledges a doctoral fellowship from CONACyT, Mexico.

Appendix A. Supplementary data

Supplementary material related to this article can be found online at https://doi.org/10.1016/j.physa.2020.125069.

References

[1] M.A. Halcrow, Spin-Crossover Materials: Properties and Applications, John Wiley & Sons, 2013.
[2] P. Gütlich, H.A. Goodwin, Spin crossover—an overall perspective, in: Spin Crossover in Transition Metal Compounds I, Springer, 2004, pp. 1–47.
[3] M.A. Halcrow, Structure: function relationships in molecular spin-crossover complexes, Chem. Soc. Rev. 40 (7) (2011) 4119–4142.
[4] D. Shriver, P. Atkins, C. Langford, Standard potentials, Inorg. Chem. (1994) B7–B17.
[5] P. Gütlich, A. Hauser, H. Spiering, Thermal and optical switching of iron (II) complexes, Angew. Chem. Int. Ed. Engl. 33 (20) (1994) 2024–2054.
[6] J. Yang, X. Tong, J.-F. Lin, T. Okuchi, N. Tomioka, Elasticity of ferropericlase across the spin crossover in the earth's lower mantle, Sci. Rep. 5 (2015) 17188.
[7] J.-F. Létard, P. Guionneau, L. Goux-Capes, Towards spin crossover applications, in: Spin Crossover in Transition Metal Compounds III, Springer, 2004, pp. 221–249.
[8] G.J. Halder, C.J. Kepert, B. Moubaraki, K.S. Murray, J.D. Cashion, Guest-dependent spin crossover in a nanoporous molecular framework material, Science 298 (5599) (2002) 1762–1765.
[9] P. Gütlich, A. Hauser, Thermal and light-induced spin crossover in iron (II) complexes, Coord. Chem. Rev. 97 (1990) 1–22.
[10] D. Chernyshov, N. Klinduhov, K.W. Törnroos, M. Hostettler, B. Vangdal, H.-B. Bürgi, Coupling between spin conversion and solvent disorder in spin crossover solids, Phys. Rev. B 76 (1) (2007) 014406.
[11] Y. Konishi, H. Tokoro, M. Nishino, S. Miyashita, Monte Carlo Simulation of pressure-induced phase transitions in spin-crossover materials, Phys. Rev. Lett. 100 (6) (2008) 067206.
[12] S.-i. Ohkoshi, K. Imoto, Y. Tsunobuchi, S. Takano, H. Tokoro, Light-induced spin-crossover magnet, Nat. Chem. 3 (7) (2011) 564.
[13] D. Pinkowicz, M. Rams, M. Misek, K.V. Kamenev, H. Tomkowiak, A. Katrusiak, B. Sieklucka, Enforcing multifunctionality: a pressure-induced spin-crossover photomagnet, J. Am. Chem. Soc. 137 (27) (2015) 8795–8802.
[14] D. Chernyshov, H.-B. Bürgi, M. Hostettler, K.W. Törnroos, Landau theory for spin transition and ordering phenomena in fe (II) compounds, Phys. Rev. B 70 (9) (2004) 094116.
[15] A.I. Nesterov, Y.S. Orlov, S.G. Ovchinnikov, S.V. Nikolaev, Cooperative phenomena in spin crossover systems, Phys. Rev. B 96 (13) (2017) 134103.
[16] C. Rodríguez-Castellanos, Y. Plasencia-Montesinos, E. Reguera-Ruiz, Spin-crossover in molecular crystals: An electron-coupled local vibrations model, Rev. Cubana Fís. 35 (2) (2018) 91–96.

[17] K. Pae, V. Hizhnyakov, Nonadiabaticity in a jahn-teller system probed by absorption and resonance Raman scattering, J. Chem. Phys. 138 (10) (2013) 104103.
[18] A. Palii, S. Ostrovsky, O. Reu, B. Tsukerblat, S. Decurtins, S.-X. Liu, S. Klokishner, Microscopic theory of cooperative spin crossover: Interaction of molecular modes with phonons, J. Chem. Phys. 143 (8) (2015) 084502.
[19] V. Hizhnyakov, K. Pae, T. Vaikjärv, Optical jahn–teller effect in the case of local modes and phonons, Chem. Phys. Lett. 525–526 (2012) 64–68, http://dx.doi.org/10.1016/j.cplett.2011.12.066, URL http://www.sciencedirect.com/science/article/pii/S0009261411015958.
[20] K. Pae, V. Hizhnyakov, Time-dependent jahn-teller problem: Phonon-induced relaxation through conical intersection, J. Chem. Phys. 141 (23) (2014) 234113, http://dx.doi.org/10.1063/1.4903814.
[21] J. Cardy, Scaling and Renormalization in Statistical Physics, Vol. 5, Cambridge university press, 1996.
[22] O.I. Utesov, S. Burdin, P. Rosa, M. Gonidec, L. Poggini, S.V. Andreev, Electric-field control of spin transitions in molecular compounds, Phys. Rev. B 100 (2019) 235126, http://dx.doi.org/10.1103/PhysRevB.100.235126, URL https://link.aps.org/doi/10.1103/PhysRevB.100.235126.
[23] P. Lunts, A.A. Patel, Many-body chaos in the antiferromagnetic quantum critical metal, Phys. Rev. B 100 (2019) 235104, http://dx.doi.org/10.1103/PhysRevB.100.235104, URL https://link.aps.org/doi/10.1103/PhysRevB.100.235104.
[24] J.Q. Toledo-Marín, I.P. Castillo, G.G. Naumis, Minimal cooling speed for glass transition in a simple solvable energy landscape model, Physica A 451 (2016) 227–236, http://dx.doi.org/10.1016/j.physa.2016.01.064, URL http://www.sciencedirect.com/science/article/pii/S0378437116001187.
[25] J.Q. Toledo-Marín, G.G. Naumis, Short time dynamics determine glass forming ability in a glass transition two-level model: A stochastic approach using kramers' escape formula, J. Chem. Phys. 146 (9) (2017) 094506, http://dx.doi.org/10.1063/1.4977517, arXiv:https://doi.org/10.1063/1.4977517.
[26] Julia, https://julialang.org/.
[27] M. Newman, G. Barkema, Monte Carlo Methods in Statistical Physics, Oxford University Press, New York, USA, 1999, (Chapter 1-4).
[28] D. Chadi, M.L. Cohen, Special points in the brillouin zone, Phys. Rev. B 8 (12) (1973) 5747.
[29] A. Huerta, G. Naumis, Relationship between glass transition and rigidity in a binary associative fluid, Phys. Lett. A 299 (5) (2002) 660–665, http://dx.doi.org/10.1016/S0375-9601(02)00519-4, URL http://www.sciencedirect.com/science/article/pii/S0375960102005194.
[30] G.G. Naumis, C. Wang, M.F. Thorpe, R.A. Barrio, Coherency of phason dynamics in fibonacci chains, Phys. Rev. B 59 (1999) 14302–14312, http://dx.doi.org/10.1103/PhysRevB.59.14302, URL https://link.aps.org/doi/10.1103/PhysRevB.59.14302.
[31] H.M. Flores-Ruiz, G.G. Naumis, J.C. Phillips, Heating through the glass transition: A rigidity approach to the boson peak, Phys. Rev. B 82 (2010) 214201, http://dx.doi.org/10.1103/PhysRevB.82.214201, URL https://link.aps.org/doi/10.1103/PhysRevB.82.214201.
[32] H.M. Flores-Ruiz, G.G. Naumis, Boson peak as a consequence of rigidity: A perturbation theory approach, Phys. Rev. B 83 (2011) 184204, http://dx.doi.org/10.1103/PhysRevB.83.184204, URL https://link.aps.org/doi/10.1103/PhysRevB.83.184204.